

THE α_{ox} -HE II EW CONNECTION IN RADIO-LOUD QUASARS

John Timlin,¹ Shifu Zhu,¹ W. N. Brandt,¹ and Ari Laor²

¹*Department of Astronomy & Astrophysics, 525 Davey Lab, The Pennsylvania State University, University Park, PA 16802, USA*

²*Physics Department, Technion, Haifa 32000, Israel*

Keywords: Radio loud quasars (1349), X-ray quasars (1821), Quasars (1319)

ABSTRACT

Radio-loud quasars (RLQs) are known to produce excess X-ray emission, compared to radio-quiet quasars (RQQs) of the same luminosity, commonly attributed to jet-related emission. Recently, we found that the He II EW and α_{ox} in RQQs are strongly correlated, which suggests that their extreme-ultraviolet (EUV) and X-ray emission mechanisms are tightly related. Using 48 RLQs, we show that steep-spectrum radio quasars (SSRQs) and low radio-luminosity (L_{R}) flat-spectrum radio quasars (FSRQs) follow the α_{ox} -He II EW relation of RQQs. This suggests that the X-ray and EUV emission mechanisms in these types of RLQs is the same as in RQQs, and is not jet related. High- L_{R} FSRQs show excess X-ray emission given their He II EW by a factor of ≈ 3.5 , which suggests that only in this type of RLQ is the X-ray production likely jet related.

THE HE II AND α_{ox} PROPERTIES OF RLQS

RLQs comprise ≈ 10 -20% of the total quasar population, are generally more X-ray luminous than their RQQ counterparts, and typically exhibit a flatter X-ray-to-optical spectral slope (α_{ox}).¹ Zhu et al. (2020) (hereafter, Z20) studied the joint radio, optical, and X-ray luminosities of a large, optically selected sample of typical RLQs and found evidence that their X-ray emission largely originates in the corona, challenging the idea that a distinct jet component contributes substantially to the X-ray emission of typical RLQs (e.g., Miller et al. 2011). They suggested a small fraction ($<10\%$) of FSRQs (which have radio spectral slope $\alpha_r > -0.5$) may have a significant ($>30\%$) jet X-ray contribution. In a follow-up investigation of the X-ray spectral and variability properties of typical RLQs, they found that all but the most radio-luminous ($L_{\text{R}} > 10^{34.3}$ erg s⁻¹ Hz⁻¹; where L_{R} is the monochromatic 5 GHz luminosity) FSRQs had X-ray emission as would be expected from the corona (Zhu et al. 2021, submitted; hereafter Z21). Here, we provide additional evidence supporting their result.

For this investigation, we follow Timlin et al. (2021, submitted; hereafter T21) who studied the α_{ox} -He II EW relationship for RQQs. The He II emission line is a weak, high-ionization line that provides a “clean” measure of the number of EUV photons between 50–200 eV present (see Section 1 of T21). T21 found a tight correlation between α_{ox} and He II EW in RQQs, even after removing these parameters’ L_{2500} dependences, indicating that the EUV continuum is related to the X-ray emission, and possibly originates in a “warm Comptonization” coronal region. Given this tight correlation for RQQs, and that RLQ beamed jet emission is not expected to produce additional He II, investigating the α_{ox} -He II EW relation for RLQs might provide insight into the origin of RLQ X-ray emission.

Our RLQ sample was constructed using RLQs from the three quasar samples outlined in Section 2 of T21 (Just et al. 2007; SDSS-RM, Shen et al. 2019; PG, Schmidt & Green 1983). These samples were selected due to their high-quality spectral coverage of He II. In total, there are 13 RLQs from the T21 samples (1, 7, and 5 RLQs from Just et al. 2007, SDSS-RM, and PG, respectively). We also incorporated RLQs with $i < 19$ and $1.6 \leq z \leq 3.5$ from Z20 into our RLQ sample, where the brightness cut ensured that we selected the highest-quality SDSS spectra, and the redshift range ensured that He II is covered. After these cuts were imposed, 35 of the 729 quasars from Z20 were included in our sample. In total, our RLQ sample contains 48 RLQs,² of which there are 18 SSRQs ($\alpha_r \leq -0.5$), 21

Corresponding author: John Timlin
jxt811@psu.edu

¹ $\alpha_{\text{ox}} \equiv \log(L_{2\text{keV}}/L_{2500})/\log(\nu_{2\text{keV}}/\nu_{2500})$

² see <https://doi.org/10.5281/zenodo.4688086>

low- L_R ($L_R \leq 10^{34.3}$ erg s $^{-1}$ Hz $^{-1}$) FSRQs, and 9 high- L_R FSRQs, where α_r and He II EW were measured using the methods from Section 2.1.3 of Z20 and Section 3 of T21, respectively. The α_{ox} values were either adopted from Z20 or computed following Section 2 of T21.

Panels (a) and (b) of Figure 1 depict α_{ox} and He II EW as a function of L_{2500} for the SSRQs, low- L_R FSRQs, and high- L_R FSRQs, respectively. The RQQs from T21 and the best-fit relation for the RQQs from T21 are also shown. As expected, the RLQs generally exhibit larger α_{ox} values than the RQQs for a given L_{2500} . The RLQs also exhibit larger He II EW in general than their RQQ counterparts indicating the presence of a stronger EUV continuum. Panel (c) shows α_{ox} as a function of He II EW for the RLQs. Despite being more X-ray luminous and having a stronger EUV continuum, the RLQs are generally consistent with the α_{ox} -He II EW relation for RQQs. We use an Anderson-Darling two-sample test to determine if the distribution of the RQQ residuals (about the best-fit line) is consistent with those of the three RLQ sub-samples (see panel (c)). Both the SSRQ and low- L_R FSRQ distributions are statistically consistent with the distribution of RQQs, while the high- L_R FSRQ sample is not. A similar conclusion is found after removing the L_{2500} dependence of both α_{ox} and He II EW in panel (d). These panels illustrate that the EUV continuum of SSRQs and low- L_R FSRQs strongly correlates with the X-ray emission, and that the correlation is similar to the correlation for RQQs, consistent with the idea that both the X-ray and EUV photons largely originate in a similar region as for RQQs. On the other hand, the likely beamed high- L_R FSRQs are not consistent with the RQQs in these parameter spaces, probably due to a significant jet X-ray contribution as suggested in Z21. Finally, RLQs tend to have excess EUV emission compared to RQQs, at a given L_{2500} (panel b), which may indicate that a more powerful accretion-disk corona is associated with jet formation.

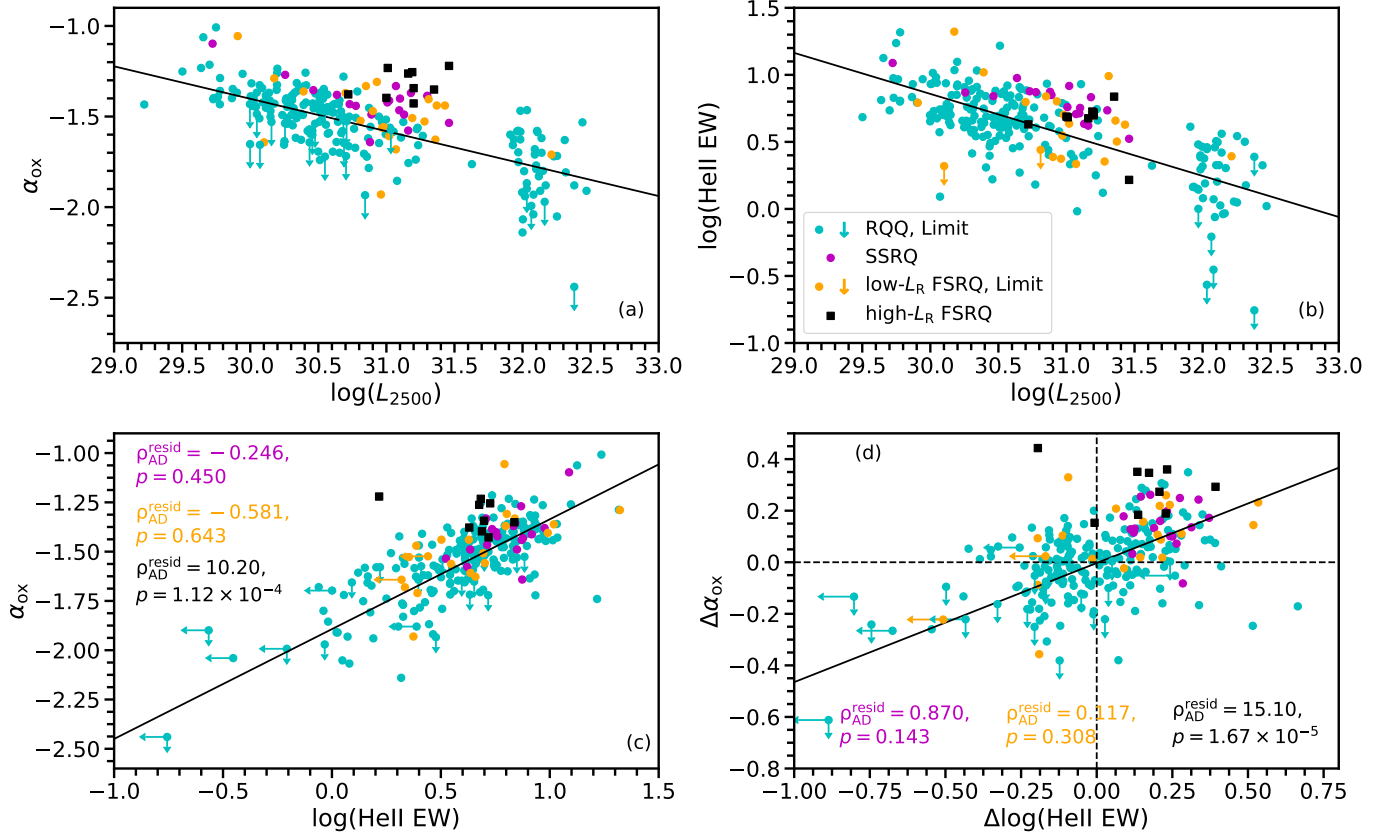


Figure 1. Panel (a): α_{ox} as a function of L_{2500} for RQQs (light blue, from T21) and the SSRQs (purple points), low- L_R FSRQs (orange points), and high- L_R FSRQs (black squares). The solid black line shows the best-fit relationship in this parameter space for the RQQs (from T21). As expected, all three radio sub-samples generally have flatter α_{ox} values than the RQQs at a given L_{2500} indicating that the RLQs generally exhibit stronger X-ray emission than the RQQs. Panel (b): The He II Baldwin effect for the RQQs and the RLQ sub-samples. As in the previous panel, all three RLQ sub-samples generally exhibit larger He II EW than the RQQs for a given L_{2500} value. Panel (c): The relationship between α_{ox} and He II EW for both the RQQs and RLQ sub-samples. The α_{ox} values of the SSRQs and the low- L_R FSRQs are well described by the best-fit relationship for the RQQs despite being both more X-ray luminous and having a stronger He II ionizing continuum, whereas the high- L_R FSRQs deviate significantly from this relationship. We quantify this using the distributions of the residuals about the best-fit line for the RQQs (black line). Anderson-Darling two-sample tests are performed between the RQQ residual distribution and the residual distributions of the three RLQ sub-samples (the results are listed in the Figure for each RLQ sub-sample by their respective color). The similarity between the residuals of the RQQs and the SSRQs and low- L_R FSRQs indicates that the X-ray emission of these two RLQ populations largely originates in the corona; however, the RQQ and the high- L_R FSRQ residual distributions are not consistent, which suggests that a jet X-ray component is likely present in these quasars (e.g. Z21). Panel (d): Similar to panel (c), but we remove the L_{2500} dependence of both α_{ox} and He II EW shown in panels (a) and (b). The AD tests of the residual distributions show a similar result as in panel (c). These panels together demonstrate that the He II ionizing continuum is related to the coronal emission in both RLQs and RQQs even after removing the effects of L_{2500} , and that the X-ray emission from typical RLQs largely originates in the corona.

REFERENCES

- Schmidt, M. & Green, R. F. 1983, *ApJ*, 269, 352.
doi:10.1086/161048
- Kellermann, K. I., Sramek, R., Schmidt, M., et al. 1989, *AJ*, 98, 1195. doi:10.1086/115207
- Just, D. W., Brandt, W. N., Shemmer, O., et al. 2007, *ApJ*, 665, 1004. doi:10.1086/519990
- Miller, B. P., Brandt, W. N., Schneider, D. P., et al. 2011, *ApJ*, 726, 20. doi:10.1088/0004-637X/726/1/20
- Shen, Y., Hall, P. B., Horne, K., et al. 2019, *ApJS*, 241, 34. doi:10.3847/1538-4365/ab074f
- Timlin, J. D., Brandt, W. N., Laor, A. 2021, *MNRAS*,
Manuscript submitted for publication. (T21)

Zhu, S. F., Brandt, W. N., Luo, B., et al. 2020, MNRAS, 496, 245. doi:10.1093/mnras/staa1411 (Z20)

Zhu, S. F., Timlin, J. D., Brandt, W. N. 2021, MNRAS, Manuscript submitted for publication. (Z21)

SUPPLEMENTARY MATERIAL

In this Section, we provide some supplementary Figures and describe in more detail the columns in our data table. In Figure 2, we depict the residual distributions of the α_{ox} –He II EW parameter space (left panel) and the $\Delta\alpha_{\text{ox}}$ – Δ He II EW parameter space (right panel). As presented above, the SSRQ and low- L_{R} FSRQ distributions are consistent with the RQQ distribution in these parameter spaces, and the high- L_{R} FSRQ distribution is clearly offset from zero residual in both cases. The mean of the high- L_{R} FSRQ residual distribution in the α_{ox} –He II EW parameter space is 0.21, which indicates that the mean X-ray luminosity of these quasars is ≈ 3.5 times larger than expected from the He II EW of the RQQs. The mean residual α_{ox} values of the SSRQ and low- L_{R} FSRQ distributions are 0.03 and 0.04, respectively. All three RLQ sub-samples have a similar deviation about their mean of ≈ 0.12 ; thus, the high- L_{R} FSRQ distribution is the only one not consistent with zero residual.

In Figure 3 we reproduce panels (b)–(d) from Figure 1, however we now investigate the relationships with respect to C IV EW instead of He II EW. In panel (a) of Figure 3 we find that the C IV EW for RLQs is generally larger than the expected value for RQQs at a given L_{2500} as is the case with He II EW, again indicating that the EUV emission in RLQs tends to be stronger than in RQQs. We depict the α_{ox} –C IV EW relation and the $\Delta\alpha_{\text{ox}}$ – Δ C IV EW relation in panels (b) and (c), respectively. In both panels (b) and (c), the $\alpha_{\text{ox}}/\Delta\alpha_{\text{ox}}$ values of the SSRQ and low- L_{R} FSRQ populations appear to be slightly more offset at a given C IV EW than was found using He II EW. As before, we use the Anderson-Darling two-sample test to compare the residual distributions of the RLQ populations with that of the RQQs. In both panels, the residual distributions of the high- L_{R} FSRQs still exhibit a more striking statistical difference from the distribution of the RQQs than the SSRQs and the low- L_{R} FSRQs, though the p -values for the latter two populations are smaller than what was found using He II. These decreases may be due to the environmental effects of the quasar on C IV EW that do not significantly affect the He II EW (see Section 1 of T21 for further discussion), though more data are required to perform a more detailed investigation. In both panels (b) and (c), the spread of the SSRQs and low- L_{R} FSRQs are consistent with zero residual whereas the high- L_{R} FSRQs are still significantly offset.

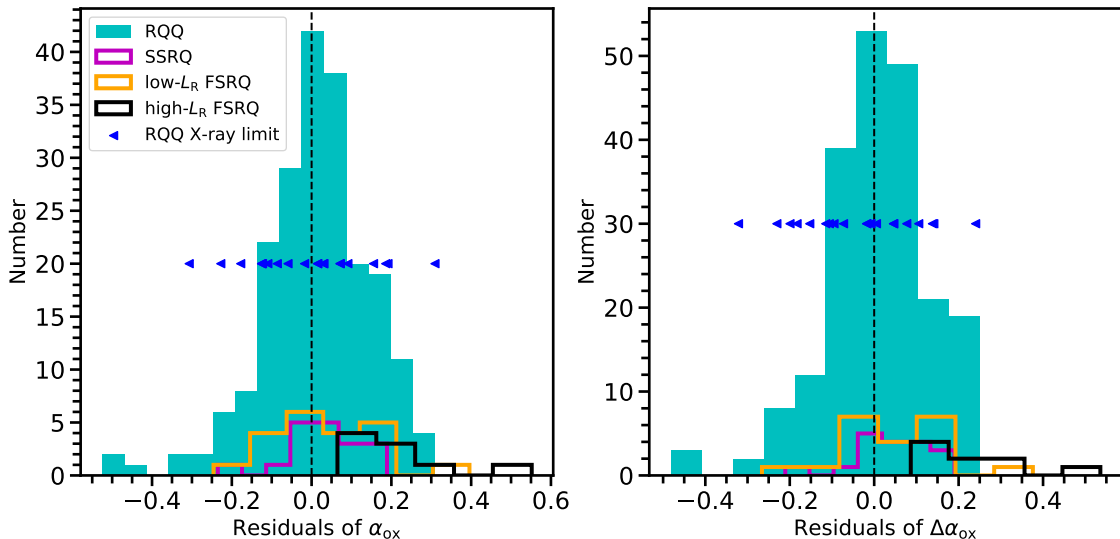


Figure 2. The left-hand and right-hand panels depict the residual distributions from panels (c) and (d) in Figure 1, respectively. Clearly, in both panels, the high- L_{R} FSRQs are offset with respect to the other distributions. Note, all RLQs investigated are X-ray detected.

Finally, we report the relevant multi-wavelength information for each of the 48 RLQs used in this work (see the associated Table). The first four columns of this table report the name of the sample from which the RLQ was drawn, the ID given to the quasar in that sample, and the RA and DEC (in decimal degrees) of each object. The redshift and the SDSS i -band magnitude (where applicable) are provided in columns (5) and (6). Columns (7)–(9) report the logarithm of the 2500 Å, 5 GHz, and 2 keV luminosities (all in units of $\text{erg s}^{-1} \text{Hz}^{-1}$). The logarithm of the radio-loudness parameter is provided in column (10) and the radio spectral slope in column (11). Column (12) reports

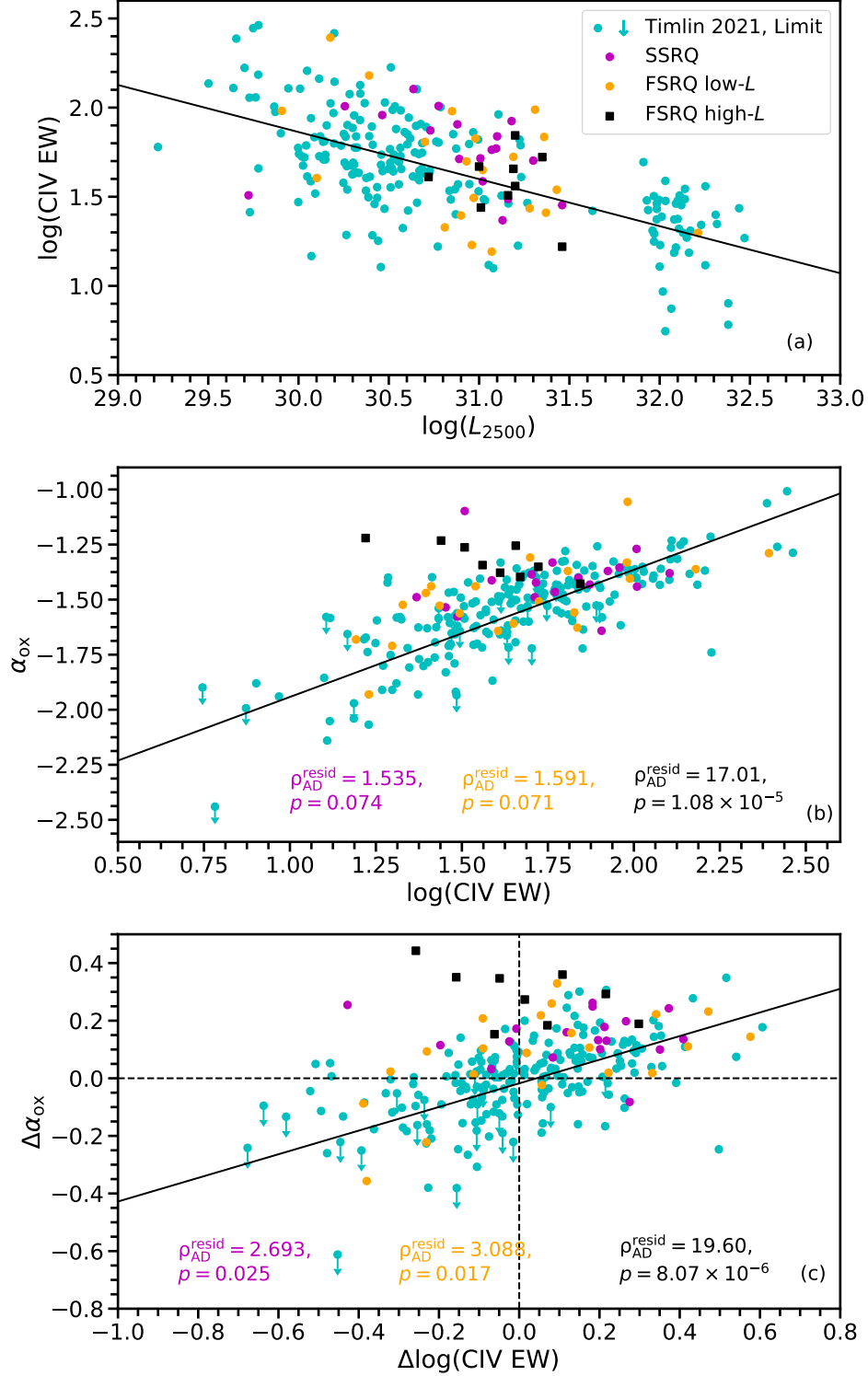


Figure 3. Similar to panels (b)–(d) in Figure 1, however we now depict C IV EW instead of He II EW. Panel (b) demonstrates that the RLQs generally have a stronger C IV EW than the RQQs, however the offset is not as clear as for He II EW. Panels (c) and (d) also show that the SSRQs and the low- L_R FSRQs are slightly more offset from the RQQs in these parameter spaces than their He II EW counterparts in Figure 1. As before, we quantify the consistency of the residual distributions of the RQQs with the SSRQs, low- L_R FSRQs, and high- L_R FSRQs using the Anderson-Darling two-sample test. We find that the residual distributions of the SSRQs and low- L_R FSRQs have a slightly lower p -value in this C IV EW parameter space than in the He II EW parameter space, which may be due to the effects of the quasar environment on the C IV EW that do not materially affect the He II EW. The high- L_R FSRQs remain strikingly inconsistent from the RQQs, indicating that their X-ray emission likely has a jet-linked contribution.

the α_{ox} value from either Z20, or computed following Section 2 of T21. Finally, in Columns (13)–(15) we report whether the He II emission line was detected in the spectrum, the logarithm of the rest-frame He II EW (in \AA), and the logarithm of the rest-frame C IV EW (in \AA).